Metals and Materials International
https://doi.org/10.1007/s12540-018-00228-5

Role of Heat Treatment on the Fabrication and Electrochemical Property of Ordered TiO_2 Nanotubular Layer on the As-Cast NiTi

Fatemeh Mohammadi[1] · Mahshid Kharaziha[1] · Ali Ashrafi[1]

Received: 23 August 2018 / Accepted: 27 November 2018

Abstract
We investigated the effect of various heat treatment processes on the formation and electrochemical properties of ordered TiO_2 nanotubes (TNTs) on NiTi. In this respect, after solution treatment of as-cast NiTi samples at 900 °C for 1 h, four different heat-treated groups were examined consisting of furnace-cooled sample, water-quenched sample, water-quenched/300 °C-aged treated (300T-NiTi) and water-quenched/500 °C-aged treated (500T-NiTi) samples. Consequently, heat-treated samples were anodized in ethylene glycol solution containing NH_4F. Results showed that the microstructure, chemical composition and grain size of the NiTi samples depended on the heat treatment process. Water-quenching and subsequent aging process provided fine precipitations distributed in the grain boundaries and reduced grain size. Furthermore, it was found that TNTs with various distributions and microstructures could be developed depending on the heat-treatment process of NiTi samples as well as anodization voltage and time. Noticeably, anodization of 500T-NiTi samples resulted in formation of well-distributed TNTs with diameters of 30 ± 5 nm. Moreover, heat-treatment process as well as TNT formation resulted in significantly enhanced corrosion resistance of as-cast NiTi substrate and reduced Ni release, depending on the treatment process. Regarding potential applications, anodization of water-quenched and 500 °C aged treated NiTi at 50 V for 10 min could provide nano-scaled biofunctional coating to promote the biological applications of NiTi implants.

Keywords Anodic oxidation · Nanotube arrays · NiTi alloy · Heat treatment process

1 Introduction

Nickel titanium (NiTi) is an intermetallic compound which derives its attractiveness from unique properties like shape memory effect, superelasticity, excellent kink resistance, constant unloading stresses, fatigue resistance and biocompatibility [1]. Moreover, the biocompatibility of NiTi makes it an ideal engineering material for medical applications including maxillofacial and dental implants, joint replacements, bone plates, bone tissue engineering and cardiovascular stents [2, 3]. The main concern of NiTi alloy is its poor corrosion resistance leading to Ni ion release [4].

It was reported that amount of released Ni ions increased with time and remained at a high level after implantation for several weeks or even several months. Excessive Ni ions could suppress cell metabolism, differentiation and proliferation and induce cell apoptosis as well as carcinogenicity though trace Ni ions are essential for human beings [4]. Moreover, the oxide layer formed on nitinol surface, spontaneously, is very thin (< 10 nm) and could not be readily repassivated once be damaged. Therefore, in order to improve the performance of NiTi alloy for biomedical applications of NiTi alloy, corrosion resistance must be enhanced and leached Ni ions from bulk materials must be inhibited [4].

Several surface modification techniques such as electrochemical treatment [5], chemical etching [6], ion implantation [7], plasma spray [8], anodization [6], laser and electron beam irradiation [9] and different coatings [5] have been applied to enhance the corrosion resistance of NiTi alloy. Among them, anodization is a simple and common method which forms nano-functional coating in various forms of TiO_2 nanotubes (TNTs) and nano-porous structure [10]. Anodization of NiTi and formation of nanotube

Electronic supplementary material The online version of this article (https://doi.org/10.1007/s12540-018-00228-5) contains supplementary material, which is available to authorized users.

✉ Mahshid Kharaziha
Kharaziha@cc.iut.ac.ir

[1] Department of Materials Engineering, Isfahan University of Technology, Isfahan 84156-83111, Iran

Published online: 07 December 2018

arrays was reported by Kim et al. [11] for the first time and, subsequently, extensive researches were carried out on the morphology of nanotubes and the factors affecting it [12–14]. For instance, Hang et al. [15] studied the effect of anodization process consisting of anodization voltage, temperature, and NH_4F concentration in the electrolyte on the TNT formation ability. In another study, Hang et al. [16] fabricated Ni–Ti–O NTs with different sizes on NiTi alloy through varying the anodization voltages and evaluated the corrosion behavior of Ni–Ti–O. They found that the corrosion resistance of the samples significantly enhanced on the large TNTs due to their high specific surface area. Furthermore, researches revealed that biocompatibility of NiTi alloy enhanced after formation of nanotubes [17, 18]. For example, it has been previously shown that TiO_2 NTs could improve osteoblast attachment, function, and proliferation [19]. Furthermore, these surfaces exhibited very low immunogenicity, eliciting low levels of monocyte activation and cytokine secretion [20]. Peng et al. [20] found that the nanotubular surface significantly enhanced proliferation of vascular cells (endothelial cells). Furthermore, TNTs with open ends may serve as carriers for deliver drug [21]. In addition, the TiO_2 and, specifically, nanocrystalline titania are attractive due to its photocatalytic activity which is hopeful to kill a wide spectrum of organisms such as cancer cells and bacteria making it promising for various biomedical applications [22–25]. Therefore, wide researches have been performed to develop nanocomposite coatings based on titania to promote antibacterial characteristics of the structures [26, 27].

Although wide researches were carried out on the formation of nanotubes on NiTi alloy, the role of the heat treatment process of cast NiTi ingots on the TNT formation has never been investigated. Results showed that heat treatment process revealed significant effects on the microstructural phases in the NiTi samples [28, 29]. In this process, exposure time, heat treatment temperature and rate of cooling could have affective role on the final microstructure and properties of Nitinol [30]. In this study, we investigated the effects of heat treatment and following cooling rate of cast Nitinol on the fabrication and morphology of TNT formation. Moreover, the effects anodization parameters on the nanotube formation on the investment cast Nitinol were studied. Finally, the corrosion behavior of anodized NiTi alloy was investigated.

2 Materials and Methods

2.1 Sample Preparation

The ingot of nickel-titanium alloy was prepared in the vacuum induction melting (IR-VAR1) via melting titanium foil (96.8% purity, Iran) and nickel ingot (97% purity, Iran). Consequently, as prepared NiTi alloys were cut into the sheets with size of 15 mm × 10 mm × 1 mm. Consequently, the samples were ground with a series of SiC papers from 180 to 2400 meshes and finally polished to finish mirror followed by ultrasonically cleaning using ultrasonic bath (Power sonic 410, activation frequency of 40 kHz, working temperature of 30–50 °C) in acetone and alcohol for 10 and 15 min, respectively. In order to provide homogeneous composition, NiTi samples were solid solution treated at 900 °C for 1 h in a vacuum tube to minimize the oxidation of the samples at high temperatures. The specimens were then cooled down to room temperature via two different cooling rates: furnace-cooling (1 °C/min) and water-quenching processes (at 35 °C). Moreover, in order to investigate the effect of aging process, two different temperatures (300 °C and 500 °C) were applied on water quenched samples. The samples were heated with rate of 8 °C/min and kept for 1 h at the mentioned temperatures and consequently cooled down with the rate of 1 °C/min. Table 1 presents the sample name applied to identify each sample.

2.2 Anodization Process of NiTi Samples

The anodization process was performed using a DC power supply (IPC-SL20200 J, 20 A, 200 V, Iran) in a two-electrode configuration with NiTi alloy as working electrode and platinum foil (10 mm × 10 mm × 1 mm) as the counter electrode, while the distance between two electrodes was set at 20 mm. Each sample was anodized in 100 mL electrolyte solution composed of ethylene glycol (Merk Co) containing 0.25 wt% NH_4F (Merk Co) and 1.5 vol% H_2O. In order to investigate the effect of heat treatment processes on the formation of TNT and structure of anodized samples, the samples were anodized at 60 V for 30 min. Consequently, in order to evaluate the role of anodization parameters on the TNT formation and its structure, the optimized heat treated sample was anodized at various voltages (25–80 V) for different times (10, 13, 15, 30 and 60 min) in the mentioned electrolyte. In order to identify the anodized samples "A" word was applied before sample name.

Table 1 Sample identification according to heat treatment parameters

Sample	Cooling environment	Temperature of aging (°C)
NT-NiTi	Non-treated	–
FC-NiTi	Furnace	–
WQ-NiTi	Water	–
300T-NiTi	Water	300
500T-NiTi	Water	500

2.3 Characterization of NiTi Samples

To investigate the influence of heat treatment and anodization process on the chemical composition of NiTi alloy, X-ray diffraction (XRD, X'Pert Pro X-ray diffractometer, Phillips, Netherlands-technique carried out with monochromatized CuKa radiation ($\lambda = 0.154$ nm) at a generator voltage of 40 kV) and Energy-dispersive X-ray spectroscopy (EDS, Philips) were performed. Moreover, the microstructure of samples, before and after anodization process, was investigated using optical microscopy (Nikon epiphot 300), scanning electron microscopy (SEM, Philips, XL30) and Field-emission scanning electron microscopy (FESEM, MIR3TESCAN-XMU). Before SEM imaging, samples were coated with a thin layer of gold via sputtering coating (Bal-Tec SCD 005). The length and diameter of nanotubes was also estimated from SEM images using Image J software. Moreover, during the anodization process, the current density was recorded using a digital multi-meter connected to a computer (MT 1860).

2.4 Corrosion Evaluation of NiTi Samples

The corrosion behavior of the anodized samples was evaluated on an electrochemical cell by potentiodynamic polarization (Potentiostat Origalys, France) in phosphate buffered solution (PBS, pH 7.4) composed of 137 mM NaCl, 2.7 mM KCl, 1.5 mM KH_2PO_4, and 8 mM Na_2HPO_4. The hardware consisted of a 20 mL three electrode cell with a Ag/AgCl as a reference electrode, platinum (Pt) foil as the counterpart and anodized sample as the working electrode. The experiments were performed at a constant temperature of 37 °C. After immersion in PBS for 4 min, the polarization curves were obtained over the potential range between − 0.7 V and 1 V at a constant scanning rate of 1 mV/s. Corrosion potentials (E_{corr}), current densities (I_{corr}), and cathodic Tafel slopes (β_c) of the samples were acquired from Tafel extrapolation method.

2.5 Ni Release from NiTi Samples

To investigate the amount of Ni released from the samples, potentiostatic polarization technique was performed on an electrochemical cell in PBS (pH = 7.4, at 37 °C). The cell consisted of three electrodes with Ag/AgCl as the reference electrode, platinum (Pt) foil as the counterpart and samples as the working electrodes. The potential was fixed at 0.3 V for 30 min. The amount of Ni released after potentiostatic polarization was investigate by Inductively coupled plasma optical emission spectroscopy (ICP/OES, 730 ES, Varian company, USA).

3 Results and Discussion

3.1 Characterization of NiTi Samples

As the microstructure of substrate has significant role on the anodizing process, the microstructure of the as-cast NiTi (NT-NiTi) was investigated. XRD pattern and the microstructure of as-cast NiTi alloy are presented at Fig. 1a, b, respectively. According to the XRD pattern, while the main phase of the as-cast sample was NiTi, the atomic segregation happed during casting leading to formation of secondary phases. NiTi substrate consisted of two main B2 austenite (00-019-0850) and B19′ martensitic (00-027-0344) phases. These phases are common in the microstructure of as-cast NiTi at room temperature [29]. Generally, as-cast NiTi alloy possesses body centered cubic (BCC) structure at high temperature [31]. Cooling to low temperature resulted in the phase transition to austenite with B2 type ordered structure. With the continuous decrease of temperature, the B2 austenite transformed into the B19′ martensitic structure [31]. Therefore, it is expected that the microstructure of as-cast NiTi made up of B2 austenite or B19′ martensite, or a mixture of the two ones, at room temperature [31]. In addition, minor phases of Ni-rich Ni_4Ti_3 and Ti–rich Ti_2Ni phases was detected. According to previous researches, the formation of the Ti_2Ni phase leads to the formation of Ni-rich matrix, after casting process the NiTi matrix to be rich in Ni [32]. These two minor phases could be detected at the microstructure of the as-cast NiTi sample in the both grains and grain boundaries (Fig. 1b). EDX spectra in three different points of NiTi substrate (Fig. 1c and Supplementary Fig. S1) clearly confirmed that the grains (point A) were rich in Ni. According to phase diagram of NiTi [33], it is expected that during solidification of binary NiTi alloys, Ti_2Ni phase forms through a peritectic reaction, $\beta + L \rightarrow \delta$ (Ti_2Ni), at 948 °C [34]. Occurrence of the Ti_2Ni phase distributing among the matrix (point B) led to formation of Ni-rich grains. Therefore, the grain boundaries and their surrounding areas (point C) were Ti–rich. EDS-map analysis of ac-cast NiTi alloy (Fig. 1d) clearly confirmed the segregation of Ni and Ti in NiTi casting.

In order to develop homogenous microstructure, heat treatment process was performed. According to the SEM images (Fig. 2) and the optical microscopy images (supplementary Fig. S2), the participates belonging to the secondary phases were observed in all figures with various distributions, depending on the heat-treatment approach. While the microstructure of as-cast sample (NT-NiTi) consisted of the inhomogeneous precipitations in whole NiTi matrix (at grain boundary and inter-boundary) (Fig. 2a and Fig. S2(a)), 1-h solution treatment at 900 °C resulted in

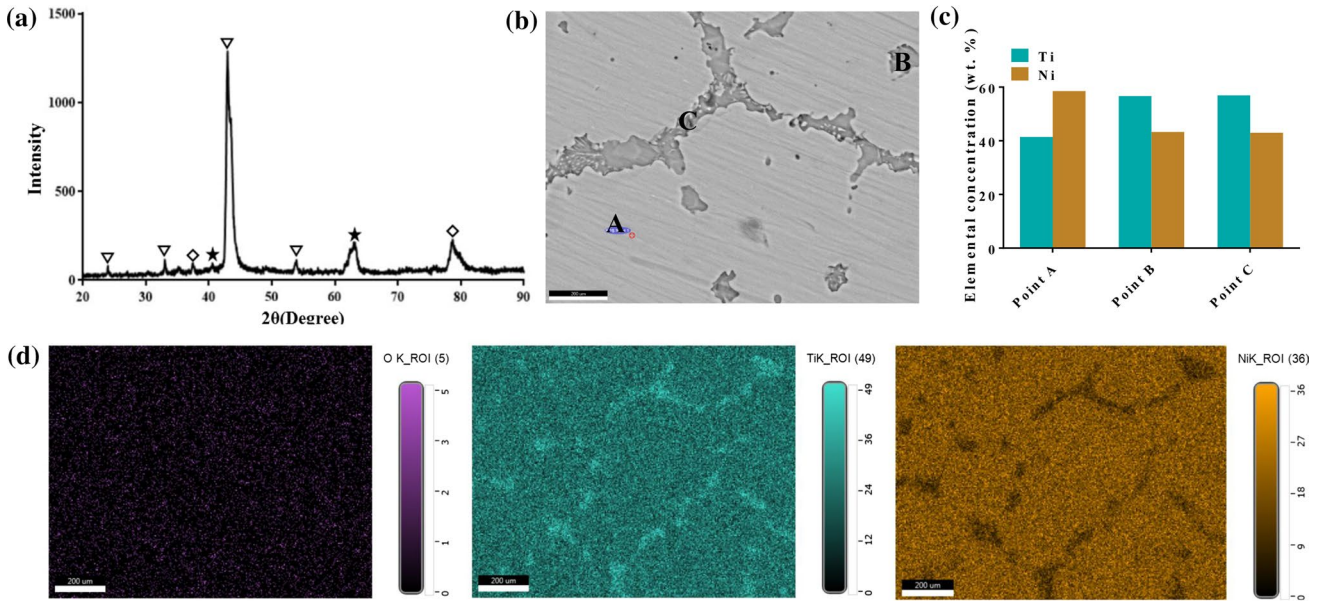

Fig. 1 (**a**) XRD pattern and (**b**) SEM micrograph of as-cast NiTi. (**c**) Elemental analysis of various points detected in section b. (**d**) EDS-map analysis of the as-cast NiTi surface

dissolution or formation of finer precipitation. When the specimens were cooled in furnace (FC-NiTi, Fig. 2b and Fig. S2(b)), precipitation could be detected on high energy regions such as grain boundaries, and interface of non-dissolved precipitations. This behavior was similarly reported in previous researches [35]. When the cooling rate was very high (WQ-NiTi, Fig. 2c and Fig. S2(c)), there was not enough time for re-precipitating within high energy zones in the cooling process. As a consequence, just some of the inter-metallic precipitates on grain boundaries with high energy, or the precipitations which had not have enough time to dissolve, remained. Aging of the water-quenched NiTi sample (WQ-NiTi) at 300°C (300T-NiTi, Fig. 2d and Fig. S2(d)) and 500 °C (500T-NiTi, Fig. 2e and Fig. S2(e)) resulted in formation of more uniform structure with fine precipitation at grain boundaries. The average grain size of various samples estimated from optical microscopy images (Supplementary Fig. S2(f)) revealed that during quenching process, the grains become clustered and finer grain structure was observed at WQ-NiTi (93.87 ± 18.32 µm) vs at NT-NiTi (149.149 ± 21.22 µm) and at FC-NiTi (158.63 ± 25.42 µm). These clustering could be produced by the loss of vacancies [36]. Robertson et al. [37] investigated the effect of heat treatment on the microstructure of Nitinol and reported grain growth during slow cooling process (such as furnace cooling process in this study). However, aging treatment of the water-quenched NiTi sample (WQ-NiTi) at 300 °C and 500 °C did not significantly change the grain size. Miyazaki and coworker [38] reported that secondary heat treatment such as aging in 300–500 °C could change significantly the microstructure of NiTi alloy.

XRD patterns of all samples (Fig. 2f) revealed that, after heat-treatment process, Ni_4Ti_3 was removed after solution treatment, while Ti_2Ni phase still remained. According to the equilibrium diagram of Ti-Ni system [39], Ti_2Ni is thermodynamically stable above 900 °C, while Ni_4Ti_3 is metastable under the same temperature. Cheng et al. [40] treated NiTi alloy at 1050 °C for different times. They found that the solution treatment at 1050 °C did not have significant effect on the stable Ti_2Ni second phase, while reduced the amount of Ni_4Ti_3 phase. SEM images (Fig. 2) confirmed that Ti_2Ni phase formed on or near the grain boundaries.

3.2 Characterization of Anodized NiTi Alloy

The effect of heat treatment processes on the formation and structure of TNTs is presented in Fig. 3 and supplementary Fig. S3. The samples were anodized at 60 V for 30 min. Anodized NT-NiTi sample (A(NT-NiTi), Supplementary Fig. S3) consisted of a porous structure, owing to its inhomogeneous chemical composition preventing from the formation of TiO_2 oxide layer. El-Hadad et al. [41] anodized as-cast NiTi alloy at 10 V for 1 h and similarly reported the formation of a well-defined anodized layer containing semi-porous structure. Moreover, the surface of anodized WQ-NiTi (A(WQ-NiTi)) and 300T-NiTi (A(300T-NiTi)) samples consisted of particulate or nodular structure, while nanotubes could not be detected. In contrary, TiO_2 nanotubes were detected on anodized FC-NiTi (A(FC-NiTi))

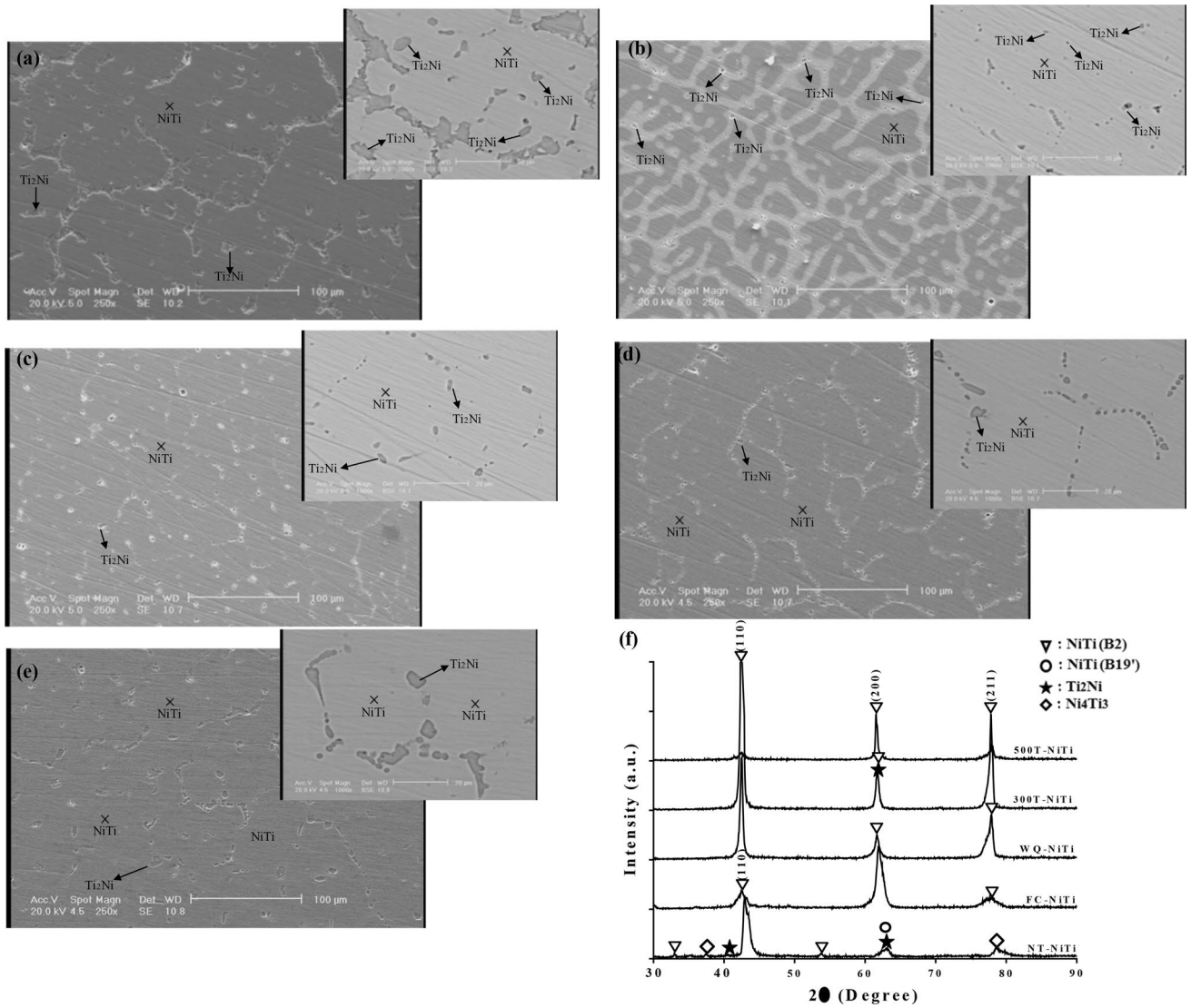

Fig. 2 SEM images of (**a**) NT-NiTi, (**b**) FC-NiTi, (**c**) WQ-NiTi, (**d**) 300T-NiTi, (**e**) 500T-NiTi sample. (inset: Higher magnification images) (**f**) XRD patterns of heat-treated samples

and 500T-NiTi (A(500T-NiTi)) samples in the form of compressed clusters which might be due to the long-time of anodizing process. Low magnification images of (A(FC-NiTi)) and (A(500T-NiTi)) samples were also showed that these TNTs could be detected at whole structure.

In order to develop anodized TNTs with appropriate morphology in whole surface, the time of anodizing process on (A(500T-NiTi)) sample was changed (10, 13, 15 and 30 min) (Fig. 4a). Low magnification images showed that increasing the anodizing time resulted in covering more surface of sample with TNTs. However, the morphology of nanotubes slightly changed from uniform and open TNTs to spikes or clusters. SEM images of the surface and cross-section of (A(500T-NiTi)) sample anodized at 60 V for 10 min (Fig. 4a, b) showed that TNTs with average diameter size of 52±10 nm and length of 250±5 nm were formed on the surface of NiTi sample. Increasing the anodization time upon 15 min resulted in growth of TNTs leading to their aggregation and formation of bundles after 15 and 30 min of anodizing process. While 10 min anodization time resulted in formation uniform and open TNTs in whole structure, increasing the anodization process for 13 min resulted in detection of both nanotubes and bundled nanotubes.

Current density curves of (A(500T-NiTi)) sample during anodizing process for various times (Fig. 4c) showed that after a short reduction in the current density, it was enhanced with increasing anodization time. It might be explained by runaway anodization at an elevated voltage, namely current self-amplification resulting from the resistance heating consequence. The resistance heating

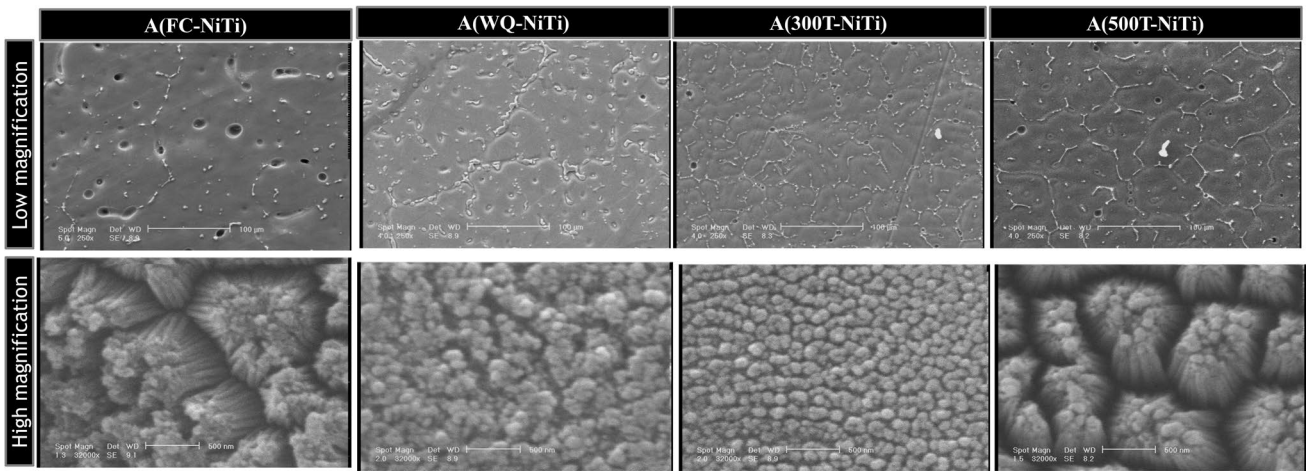

Fig. 3 SEM images of the anodized-heat treated NiTi samples at 60 V for 30 min

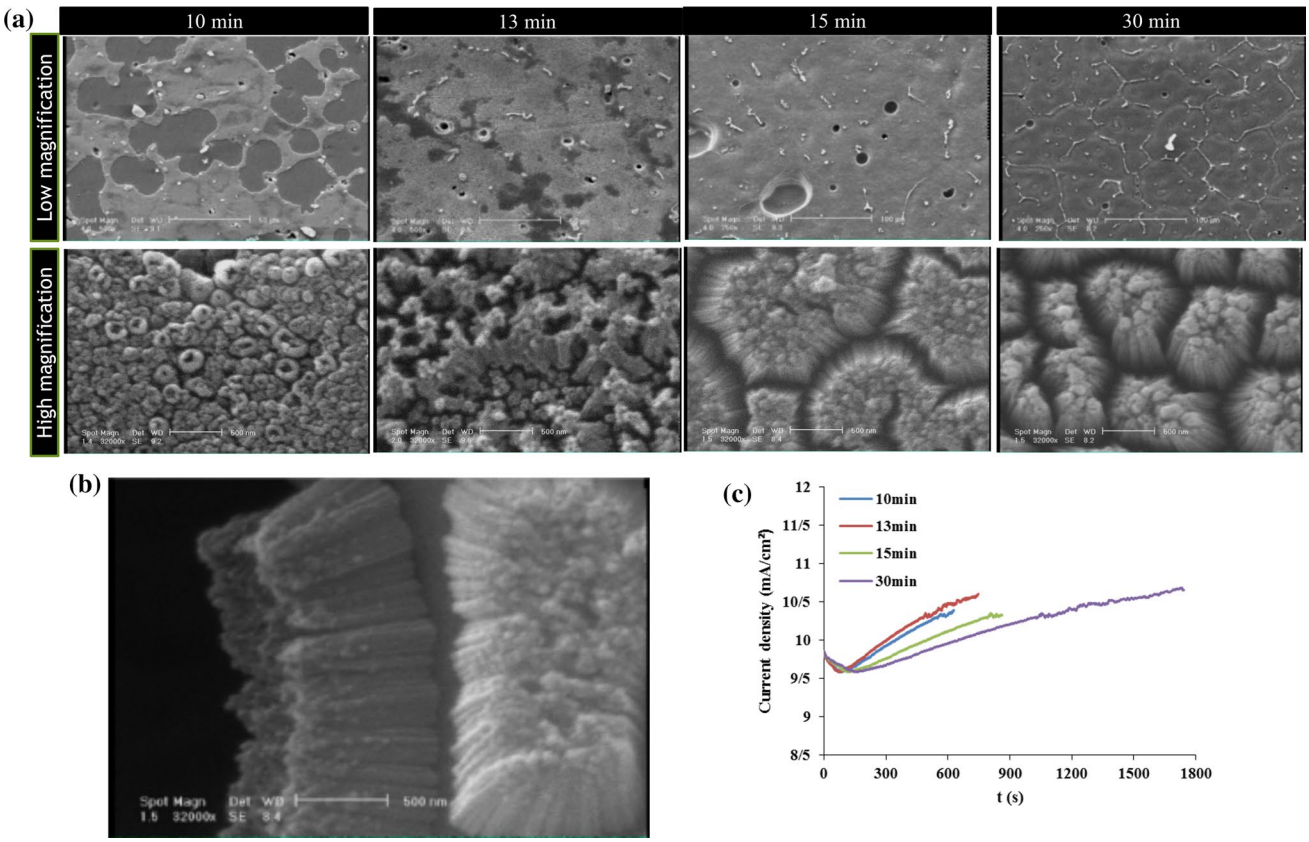

Fig. 4 SEM images of A(500T-NiTi) sample anodized at 60 V for (**a**) 10, 13, 15 and 30 min. (**b**) Cross-section image of A(500T-NiTi) sample anodized at 60 V for 10 min. (**c**) Current density-time curves of A(500T-NiTi) sample anodized at 60 V for four different times (10,13,15 and 30 min)

result enhanced the temperature of electrolyte leading to the greater electrochemical activities on the sample surface, breakdown of the oxide film and, hence, formation of micropits. The micropits acted as short-circuit channels to enhanced the current [15]. Therefore, our result confirmed that increasing anodizing time upon 10 min did not have significant positive role on the TiO_2 nanotube formation. However, according to low magnification SEM image of

10-min anodized sample, uniform nanotubes could not be formed on whole surface. It might be due to the formation of micro-pits on the surface which prevented from the formation of nanotubes completely. This result was similarly detected when anodization process was performed at 80 V.

In order to provide TNTs with optimized morphology in whole structure, anodization voltage was reduced to 25, 40 and 50 V. While TNT could not be detected at anodization voltages of 25 and 40 V, even at prolonged anodization process (data was not presented here), nanotubes could clearly be detected in whole surface, when the anodization voltage was 50 V. Figure 5 shows FESEM images at two different magnifications of heat-treated and anodized samples (A(FC-NiTi), A(WQ-NiTi), A(300T-NiTi) and A(500T-NiTi)). While nanotubes were uniformly developed on A(500T-NiTi) and A(300T-NiTi) samples, nanopores could be detected on A(FC-NiTi) and A(WQ-NiTi) samples. The diameter and distribution of these pores were depending on the heat-treatment regime. While the diameter of these pore and their distribution were non-uniform on A(FC-NiTi) sample, uniform porous structure could be identified on A(WQ-NiTi) sample. As mentioned above, cooling process in the furnace led to growth of Ti_2Ni precipitation as the second phases on high energy regions such as grain boundaries, and interface of non-dissolved precipitations, leading to formation of Ni-rich matrix. Therefore, these grains could not stimulate nanotube formation. Similarly, WQ-NiTi sample could not lead to the formation of nanotubes at this time, owing to the presence of fine precipitations in the grains. Similarly, Lozano et al. [42] anodized 6063 aluminum alloy and found that $MgSi_2$ precipitation within the matrix resulted in different electrochemical potentials between particles and matrix which made a local galvanic cell and thus causing the micro-pit formation on the surface of alloy.

SEM images of A(300T-NiTi) and A(500T-NiTi) revealed that TNTs were formed on whole surfaces. While the dimeter of TNTs formed on A(300T-NiTi) sample was 20 ± 3 nm, it was increased to 30 ± 5 nm, at A(500T-NiTi) sample (Fig. 6a). Moreover, the cross-section of A(500T-NiTi) sample (Fig. 6a) confirmed the formation of nanotubes with length of 300 ± 7 nm. Similar nanotube size was reported in previous researches studied on NiTi sample. For instance, Kim et al. [11] reported that after anodizing of commercial NiTi alloy foils for 5 min at 60 V, the average nanotube diameter was 38 nm while their length was in the range of 200–500 nm. In another research, Lee et al. [18] showed that diameter of nanotubes formed on commercial NiTi foils enhanced from 90 to 110 nm with increasing the anodization voltage from 70 to 85 V. Furthermore, the cross-section image of A(500T-NiTi) sample (Fig. 6a) showed that the side-walls of TNTs were rough, which might be due to the presence of water during anodizing process. Saharudin et al. [43] showed that increasing water content enhanced the ripple. It could be due to the mobility of H^+ which increased with high water

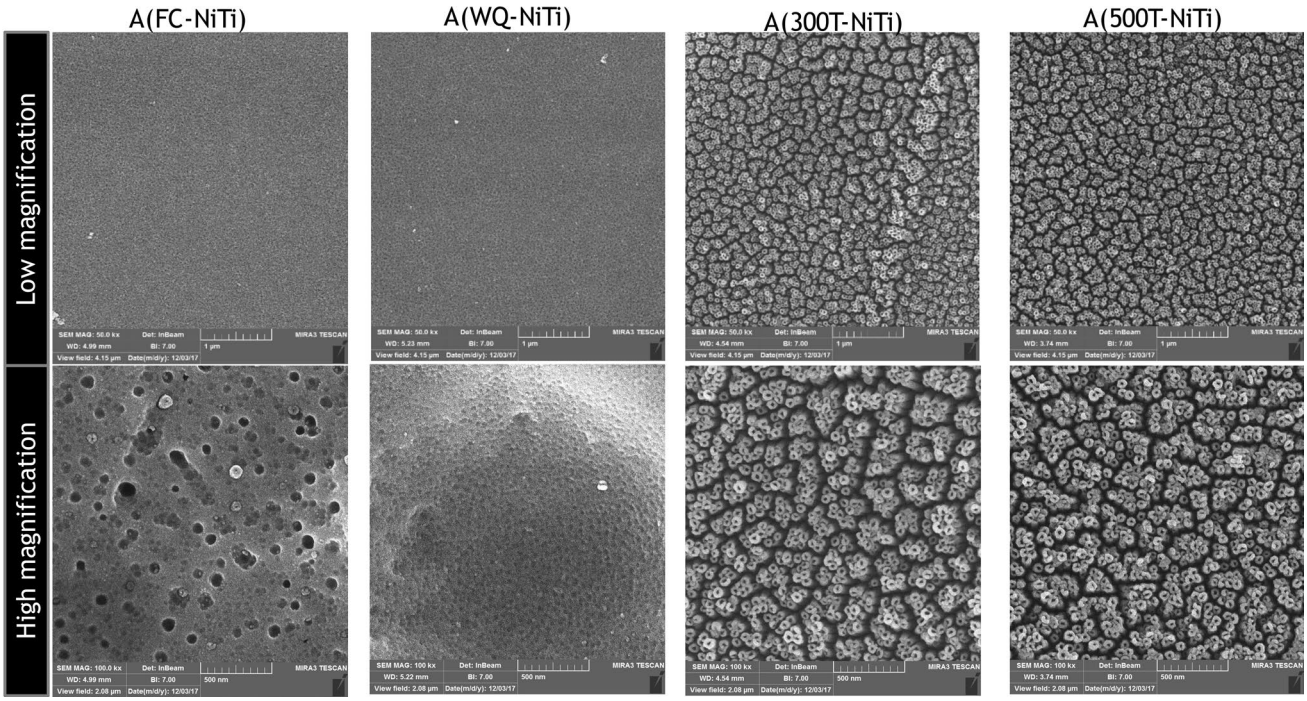

Fig. 5 FESEM images of heat treated NiTi samples anodized at 50 V for 10 min

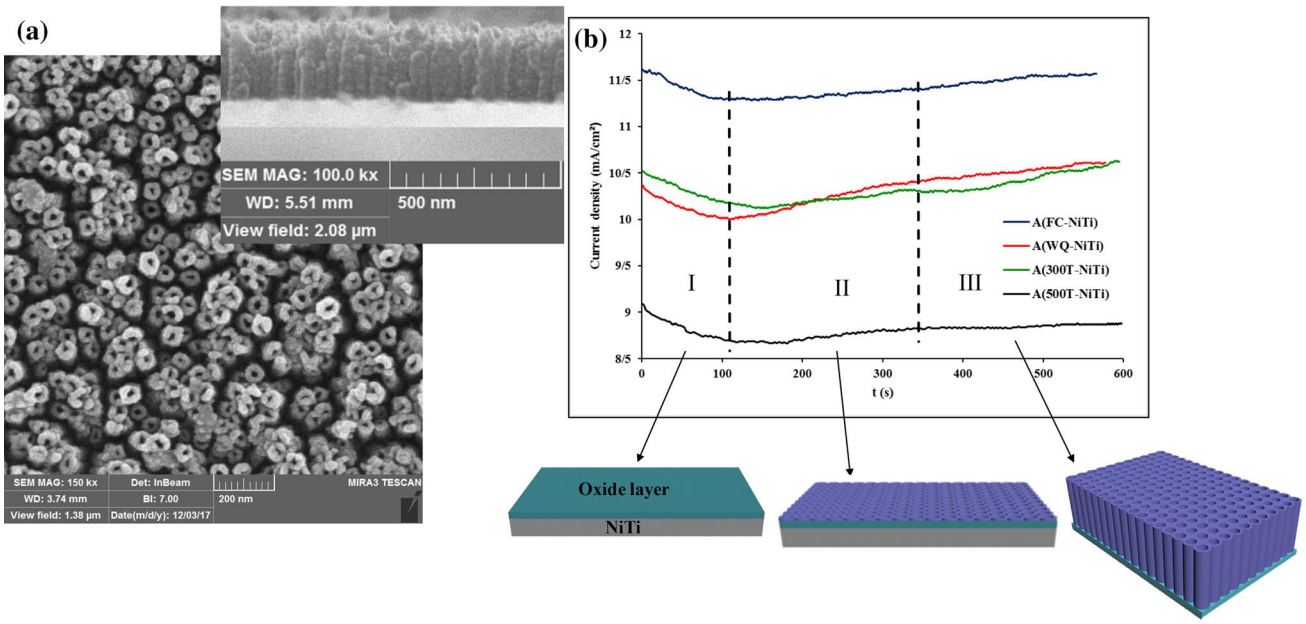

Fig. 6 (**a**) Cross-section images of 500T-NiTi sample anodized at 50 V for 10 min. (**b**) Current density curves of anodized samples (A(FC-NiTi), A(WQ-NiTi), A(300T-NiTi) and A(500T-NiTi)) at 50 V for 10 min

content, and thus change local pH value on wall of tubes, so local chemical dissolution occurs on the wall of the nanotube and ripples formed [43].

The current density-time curves of these samples during anodizing process are presented in Fig. 6b. Results showed that the anodizing process was occurred at three-step process: initially, the current density rapidly decreased when the oxide layer was formed on the metal sample. Influenced by the electrical field, O^{2-} ion species from the bulk electrolyte migrated towards the interface of the substrate-TiO_2 leading to induce the formation of barrier oxide layer (region I), Consequently, the chemical etching of the ions penetrating through the barrier oxide layer led to the formation of the small pits and pores and the slight increase in current density (region II). In the third stage (region III), the rate of oxide formation and dissolution reaction arrived to a steady-state step [44]. Moreover, our results confirmed that the current density curve of A(FC-NiTi) sample was significantly upper than others. It might be due to the presence of precipitations that made a galvanic cell and led to increase of the current density as described in previous section. Furthermore, A(500T-NiTi) sample revealed the lowest current density owing to the thicker oxide layer formed on this sample. 500T-NiTi sample consisted of the fine precipitations which distributed within the grain boundaries after aging at 500 °C.

Our results confirmed that, one step anodization at 50 V for 10 min created the appropriate morphology. Moreover, water quenching and, subsequently, aging at 500 °C could provide appropriate condition for cast NiTi to form TiO_2 nanotube on its surface.

3.3 Corrosion Behavior and Ni Release Evaluation

Potentiodynamic polarization curves of as-cast NiTi (NT-NiTi) as well as heat-treated NiTi samples anodized at 50 V for 10 min are presented in Fig. 7a and the electrochemical parameters derived from Tafel extrapolation method are listed at Table 2. Results showed that, NT-NiTi sample revealed the greatest I_{corr} (3.1×10^{-8}) compared to anodized samples, implying high corrosion tendency and rate. Moreover, between all samples, A(300T-NiTi) and A(500T-NiTi) revealed the smallest E_{corr} (−0.16 & −0.26, respectively) confirming their enhanced corrosion resistance owing to the presence of thicker oxide films than two other samples. Pourmahdavi et al. [10] reported that, compared to the bare NiTi sample, anodized NiTi revealed much higher corrosion resistance. Furthermore, Liu et al. [45] showed that anodized and mechanically polished Ti revealed better corrosion resistance than mechanically polished Ti. However, Hang et al. [16] showed that the corrosion resistance of the anodized samples decreased with increasing nanotube size. It might be due to the larger surface area in contact with the electrolyte and resulting mass transport at the electrolyte/electrode interface. Figure 7b displays the potentiostatic curves of all anodized-heat treated samples (A(FC-NiTi), A(WQ-NiTi), A(300T-NiTi) and A(500T-NiTi) as well as cast NiTi (NT-NiTi) sample. At the beginning, the current density dropped sharply to a lower level and, consequently, kept at a stable level at anodized-heat treated samples meaning the amount of released Ni reduced with increasing time. However,

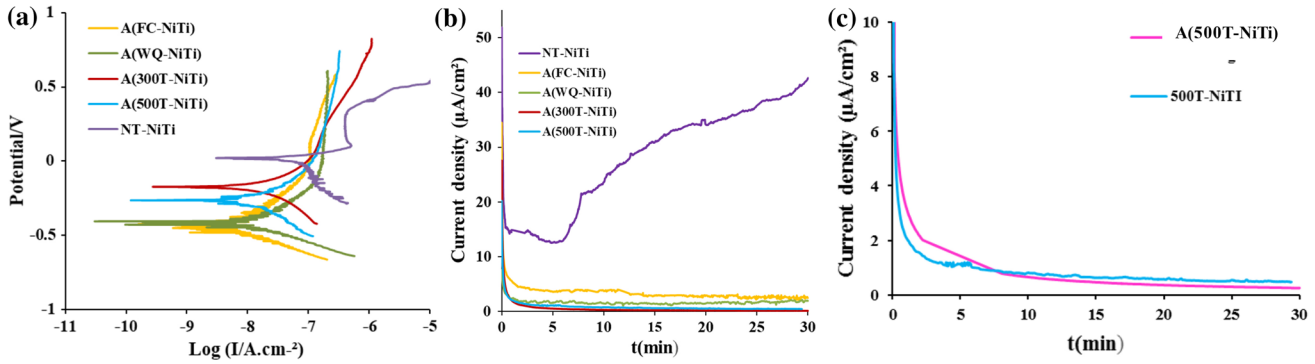

Fig. 7 (**a**) Potentiodynamic, (**b**) and (**c**) potentiostatic polarization curves of anodized-heat treated samples

Table 2 Electrochemical parameters derived from Tafel extrapolation method

Sample	E_{corr}/V versus Ag/AgCl	I_{corr}/Acm^{-2}	β_c/Vdec^{-1}
NT-NiTi	0.02	3.1×10^{-8}	0.08
A(FC-NiTi)	−0.45	0.63×10^{-8}	−0.137
A(WQ-NiTi)	−0.46	1.12×10^{-8}	−0.076
A(300T-NiTi)	−0.16	1.99×10^{-8}	−0.2
A(500T-NiTi)	−0.26	1.34×10^{-8}	−0.274

Table 3 The amounts of Ni released from various anodized samples as well as 500T-NiTi during potentiostatic test

Sample	Ni released (ppb)
NT-NiTi	85
A(FC-NiTi)	23
A(WQ-NiTi)	18
A(300T-NiTi)	9
A(500T-NiTi)	9
500T-NiTi	10

according to the potentiostatic curves of NT-NiTi, the amount of released Ni not only enhanced with increasing time, but also was significantly higher than anodized samples. It might be due to both inhomogeneous chemical composition of NT-NiTi and the thick oxide layer of nanotubes developed on anodized-heat treated samples. Moreover, between various anodized-heat treated samples, the potentiostatic curve of A(FC-NiTi) sample was upper than others showing the higher amounts of released Ni due to the presence of coarse precipitates (Ti_2Ni) in the matrix that made the matrix Ni-rich.

In order to show the role of anodizing process on the ion release, the potantiostatic curves of 500T-NiTi sample, before and after anodization process (A(500T-NiTi)) were compared (Fig. 7c). There was no significant difference between two curves in the amounts of released Ni ions confirming that heat treatment had more effective role on Ni release process. However, in another research, Hang et al. [15] investigated the amount of Ni released from NiTi before and after anodizing. They reported that the amount of released Ni from anodized NiTi was more than NiTi due to presence of NiO in the TNT layer which dissolved in the electrolyte during spontaneous electrochemical corrosion. Moreover, anodization process increases the surface area of the oxide layer due to the nanotubular structure which may be the major reason for the difference in the release of Ni.

The amount Ni ions released from anodized-heat treated NiTi samples as well as as-cast NiTi and 500T-NiTi samples are listed in Table 3. Results showed that the amount of Ni released from NT-NiTi was significantly higher than others owing to inhomogeneous composition and segregation of Ni occurring during solidification process. Heat treatment followed by anodization process revealed noticeable effect on the amount of released Ni ion. However, the amount of released Ni was much less than the tolerable limit of Ni in vivo [19] and, hence, the anodized NiTi samples should be biologically safe.

4 Conclusions

In this study, effect of various heat-treatment processes of as-cast NiTi and anodization parameters on the formation and structure of TiO_2 nanotube (TNT) were studied. While solution treatment of NiTi samples at 900 °C for 1 h and subsequently cooling at furnace resulted in elimination of some of minor phases (i.e. Ni_4Ti_3 phase) and grain growth, water quenching prevented from the growth of precipitates and reduced grain size. Moreover, aging of NiTi samples at 300 and 500 °C provided the homogenous microstructure consisting of fine precipitations distributed in the grain boundaries. Depending on the microstructures, TNTs were

formed with various morphology on the surface of NiTi. In this respect, anodization of 300T-NiTi and 500T-NiTi samples resulted in formation of well-distributed TNTs with different diameters. Moreover, anodization parameters such as voltage and time considerably affected the formation of nanotubes and their morphology. Our results confirmed that anodization of at 50 V for 10 min could provide uniform TNTs with diameters of 30 ± 5 nm and length of 300 ± 7. Furthermore, solution treatment and consequently aging at 500 °C as well as anodization process of cast NiTi could significantly reduce Ni release at physiological solutions making it promising for biomedical application such as cardiovascular stents.

References

1. F.T. Cheng, P. Shi, G.K.H. Pang, J. Alloy. Compd. **438**, 238 (2007)
2. D. Kapoor, Johnson Matthey Technol. Rev. **61**(1), 66 (2017)
3. C.W. Chan, L. Carson, G.C. Smith, Surf. Coat. Technol. **349**, 488 (2018)
4. R. Hang, X. Huang, L. Tian, Electrochim. Acta **70**, 382 (2012)
5. G. Tepe, J. Schmehl, H.P. Wendel, S. Schaffner, Biomaterials **27**, 643 (2006)
6. S. Shabalovskaya, J. Anderegg, J. Humbeeck, Acta Biomater. **4**, 447 (2008)
7. A. Shanaghi, P.K. Chu, Surf. Coat. Technol. (2018) (**in press)**
8. Z. Shi, J. Wang, Z. Wang, Y. Qiao, T. Xiong, Y. Zheng, Coatings **8**(10), 346 (2018)
9. S.N. Meisner, I.V. Vlasov, E.V. Yakovlev, S.V. Panin, L.L. Meisner, F.A. D'yachenko, Mater. Sci. Eng., A **740–741**, 381 (2019)
10. M. Pourmahdavi, N. Parvin, Adv. Mater. Res. **829**, 431 (2014)
11. J.-H. Kim, K. Zhu, Y. Yan, C.L. Perkins, A.J. Frank, Nano Lett. **10**, 4099 (2010)
12. R. Hang, M. Zong, L. Bai, Electrochem. Commun. **71**, 28 (2016)
13. Ch. Huang, Y. Xie, L. Zhou, H. Huan, Smart Mater. Struct. **18**, 024003 (2009)
14. G. Hou, Y. Xie, L. Wu, Int. J. Hydrogen Energy **41**, 9295 (2016)
15. R. Hang, Y. Liu, L. Zhao, A. Gao, L. Bai, X. Huang, X. Zhang, B. Tang, P.K. Chu, Sci. Rep. **4**, 1 (2014)
16. R. Hang, Y. Liu, S. Liu, L. Bai, A. Gao, X. Zhang, X. Huang, B. Tang, P.K. Chu, Corros. Sci. **103**, 173 (2016)
17. S.C. Roy, M. Paulose, C.A. Grimes, Biomaterials **28**, 4667 (2007)
18. P. Lee, Al. Cerchiari, T.A. Desai, Nano Lett. **14**, 5021 (2014)
19. F. Nasirpouri, I. Yousefi, E. Moslehifard, J. Khalil Allafi, Surf. Coat. Technol. **315**, 163 (2017)
20. L. Peng, M.L. Eltgroth, T.J. LaTempa, Biomaterials **30**, 1268 (2009)
21. M. Sinn Aw, K. Gulati, D. Losic, J. Biomater. Nanobiotechnol. **2**, 477 (2011)
22. S. Rana, J. Rawat, M.M. Sorensson, R.D.K. Misra, Acta Biomater. **1**, 691 (2006)
23. B.K. Sunkara, R.D. Misra, Acta Biomater. **4**(2), 273 (2008)
24. S. Ranaab, J. Rawatab, M.M. Sorenssonac, R.D.K. Misra, Acta Biomater. **2**(4), 421 (2006)
25. R. Shohal, M.M. Sorensson, R.S. Srivastava, R.D.K. Misra, Mater. Sci. Eng., B **119**(2), 144 (2005)
26. R. Venkatasubramanian, R.S. Srivastava, R.D.K. Misra, Mater. Sci. Technol. **24**, 589 (2013)
27. S. RanaR, D.K. Misra, Appl. Mater. Sci. Eng. **57**, 65 (2005)
28. K.W.K. Yeunga, K.M.C. Cheunga, W.W. Lua, C.Y. Chun, Mater. Sci. Eng. **383**, 213 (2004)
29. A. Etaati, A. Shokuhfar, E. Omrani, P. Movahed, H. Bolvard, Defect Diffus. Forum **297**, 489 (2010)
30. M. Paryab, A. Nasr, O. Bayat, V. Abouei, A. Eshraghi, Assoc. Metall. Eng. Serbia **16**, 123 (2010)
31. J. Shu-yong, Z. Yan-qiu, F. Hong-tao, Trans. Nonferrous Met. Soc. China **22**, 1401 (2012)
32. J. Shu-yong, Z. Yan-qiu, Trans. Nonferrous Met. Soc **22**, 90 (2012)
33. T.B. Massalski, H. Okamoto, P.R. Subramanian, L. Kacprzak (Eds.), Binary alloy phase diagrams, 2nd edition, vol 3 (Materials Park, OH: ASM International), p. 2874 (1990)
34. J. Bhagyaraj, K.V. Ramaiah, C.N. Saikrishna, Alloys Compd. **735**, 1145 (2013)
35. E. Omrani, A. Shokuhfar, A. Etaati, A. Dorri, A. Saatian, Defect Diffus. Forum **297–301**, 344 (2010)
36. J. Ridhwan, M. Syafiq, M.H.M. Hafidza, J. Mech. Eng. Technol. **6**, 87 (2014)
37. S.W. Robertso, X.Y. Gong, J. Mater. Sci. **41**, 621 (2006)
38. A.R. Pelton, J. DiCello, S. Miyazaki, Min. Invas. Ther. Allied Technol. **9**(1), 107 (2000)
39. K. Otuka, X. Ren, Mater. Sci. **50**(5), 511 (2005)
40. C. Cheng-lin, C. Jonathan-CY, C. Paul-K, Trans. Nonferrous. Met. Soc. **16**, 49 (2006)
41. ShH El-Hadad, K. Ibrahim, L. Wagner, Hindawi Publishing Corporation, J. Metall. **20**, 1 (2014)
42. J.A. Lozano, B.S. Peña, G.F. Vander Voort, Materials **7**, 4224 (2014)
43. S. Yoriya, W. Kittimeteeworakul, N. Punprasert, J. Chem. Chem. Eng **6**, 686 (2012)
44. K.A. Saharudin, S. Sreekantan, Adv. Mater. Res. **173**, 102 (2011)
45. Ch. Liu, Y. Wang, M. Wang, W. Huang, P.K. Chu, Surf. Coat. Technol. **206**, 63 (2011)